ACS APPLIED ENERGY MATERIALS

www.acsaem.org

Article

Benchmarking Performance and Degradation of Pt Supported on Different Carbons for PEMFC Applications Using Gas Diffusion Electrode Half-Cell

Pascal Lauf,* A. Lucía Morales, Konrad Ehelebe, Andreas Hutzler, Karl J. J. Mayrhofer, Vicent Lloret, and Serhiy Cherevko*

Cite This: ACS Appl. Energy Mater. 2025, 8, 7939−7947

Read Online

ACCESS | Metrics & More | Article Recommendations | Supporting Information

ABSTRACT: The performance of platinum nanoparticles in proton exchange membrane fuel cells (PEMFCs) depends on carbon support. In comparison to nonporous supports (Vulcan, Pt/V), porous supports (Ketjenblack, Pt/KB) reveal higher tolerance toward the decrease in the electrochemical active surface area (ECSA), which could be attributed to suppressed dissolution (net mass loss). However, distinguishing between different degradation mechanisms is challenging in membrane electrode assembly (MEA) tests. This study uses the gas diffusion electrode (GDE) half-cell setup to gain fundamental insights into the degradation of Pt/C. Several metrics are considered to benchmark GDE to MEA. First, we confirm that the optimal ionomer to carbon (I/C) ratios for Pt/V and Pt/KB of 0.65 and 1.0 are similar in both setups. The beginning of life (BOL) performance reveals that Pt/KB suffers from mass transport losses in the high current density region going up to 2 A cm^{-2}. Further, an accelerated stress test (AST) consisting of 5000 potential cycles shows a decrease in ECSA for Pt/V of ∼40% and Pt/KB of ∼30%. Quantifying Pt dissolution during the AST using online inductively coupled plasma mass spectrometry (ICP−MS), similar for all studied catalyst layers, we conclude that, for the chosen AST protocols in this study, Ostwald ripening is the dominating degradation process in both supports.

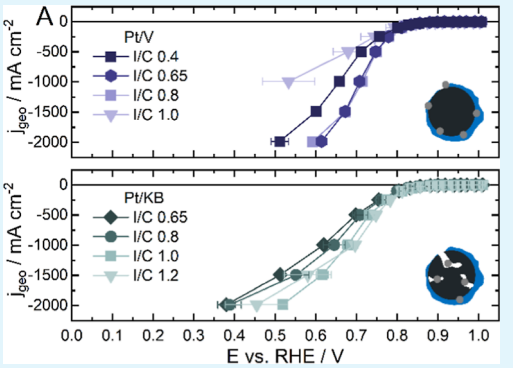

KEYWORDS: *GDE half-cell, fuel cell, platinum, Pt/V, Pt/KB, dissolution*

1. INTRODUCTION

Since the Paris Climate Conference 2015, considerable attempts have been directed toward reducing carbon dioxide generation.[1] While significant progress has been achieved over the past decade, transportation, which contributes a large part to emissions, still lags behind other energy sectors. A promising way of decarbonizing this sector is through using hydrogen fuel in proton exchange membrane fuel cells (PEMFC).[2] Although these fuel cells have already been commercialized, and the passenger car segment is projected to be one of the largest growing markets for fuel cells in the upcoming decades, research advancements and cost reductions are required to achieve widespread use of PEMFCs in the automotive industry.[3]

A large fraction of the cost of the fuel cell comes from platinum, the state-of-the-art catalyst for the sluggish oxygen reduction reaction (ORR).[4] Different material science approaches have been introduced to minimize Pt utilization while still reaching the required performance metrics, like modifying the nanoparticle's (NP) shape, introducing other metals, or applying the catalyst onto various supports and finely dispersing it on the surface of the substrate.[4,5] However, factors that are difficult to study in model systems like rotating disk electrode (RDE), i.e. Pt loading,[6] the ionomer content,[7−9] the distribution of the platinum on its supports[10] or the support itself[11,12] change the catalyst behavior in real systems. In PEMFCs, a complex interplay of Pt NPs, carbon support, and the ionomer attributed to new properties at the triple phase interface (TPI) must be considered. A representative example is the application of different carbon supports, such as activated carbon, carbon black, graphite, and graphitized structures, allowing fine-tuning of Pt NP and, hence, activity and stability.[13] Nonporous (Vulcan) and porous (Ketjenblack) are the most studied supports in both RDE and PEMFC literature.[12]

RDEs, the workhorse in fundamental electrocatalysis evaluation, have the advantage that experiments can be carried

Received: January 21, 2025
Revised: May 15, 2025
Accepted: May 19, 2025
Published: June 6, 2025

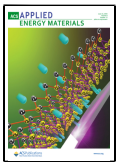

out quickly, only small quantities of material are required, and the equipment is quite affordable for laboratories.[4,14] However, the electrode architecture and electrolyte do not correspond to that used in the application, meaning that only low current densities can be achieved. In more applied research, membrane electrode assemblies (MEAs) are tested in single cells, resembling those used in fuel cell stacks. A major problem here, however, is that the electrochemical measurements have many variables, the equipment is expensive, and most of the existing external analyses are only possible post-mortem.[14] One option to bridge this gap between RDEs and MEAs is the application of floating electrode and GDE half-cell setups.[15−23]

With GDE half-cell setups, the aim is to use the advantage of a system that offers an accelerated study of catalyst layers (CLs), achieving high current densities and benefiting from coupling to external in situ and operando analyzers.[16,24] In the past few years, these GDE half-cells have been commercialized, compared in an interlab comparison,[16] coupled to external analysis,[24] and new methods from application-oriented research have been established along with various accelerated stress tests (ASTs).[25] In addition, various best practice papers were published, as well as pitfalls and the influence on the activity of catalyst structures.[16,19,26]

When considering Pt/C catalysts for PEMFC, optimization of both catalyst and support is required. Depending on the operation conditions, either Pt or C degradation can be responsible for the overall performance deterioration. However, identifying the different degradation mechanisms of Pt/C, namely carbon corrosion, platinum dissolution, Ostwald ripening, agglomeration, and particle detachment, is challenging in MEA studies.[27−29] Even though electrochemical investigations like performance, impedance, and evaluation of the electrochemical surface area (ECSA) at different humidities combined with post-mortem analysis provide a quite good investigation of single-cell tests,[30] fundamental understanding of the processes at the surface is still required. In most cases, the degradation in MEAs is characterized by ex-situ methods or visualization techniques. Rarely, in situ techniques like monitoring water in a running PEMFC, from optical photography and magnetic resonance imaging (MRI) to neutron and synchrotron X-ray imaging are used.[29] Nevertheless, these techniques mainly provide qualitative information about water's temporal and spatial distribution inside a running fuel cell. Recently, it was shown that catalyst dissolution can be studied in GDE half-cell setups.[24,31] However, less attention has been paid to the investigation of the influence of carbon support on the performance and stability of Pt/C catalysts in GDE setups, with only Vulcan carbon support studied.[31]

Recent publications from Della Bella et al.[30] and Lazaridis et al.[32] have shown that the optimization and investigation of new supports is a current topic, aiming to combine the advantages of a Pt/V and Pt/KB. Independent of the carbon support, Pt band formation caused by Pt dissolution and redeposition inside the membrane after an AST seems to occur in all cases.[11,30] Additionally, various literature uses Vulcan and Ketjenblack supports as benchmarks and references, creating reliable and comparable data in MEAs.[11,12,30,32] The systematic understanding of these different carbon supports will lead to distinct conclusions to help researchers gain a better understanding of carbon materials and modify the synthesis approaches to promising new catalysts. Nevertheless, especially these fundamental studies as well as catalyst specific properties need to be investigated more thoroughly.

In this study, we show optimization and comparison of 20 wt % Pt on Vulcan (Pt/V) and 20 wt % Pt on Ketjenblack (Pt/KB) catalysts using a GDE half-cell setup. Moreover, we investigate the degradation processes analyzing catalyst dissolution by coupling the GDE half-cell with an inductively coupled plasma mass spectrometer (ICP−MS). The successful optimization, comparison of the catalysts, and fundamental analysis of the degradation and stability of these catalysts lead to an assessment of the results and their relation to other research findings in the literature.

2. EXPERIMENTAL SECTION

2.1. Electrode Manufacturing. The CLs were produced via ultrasonic spray coating in similar conditions to those described in our earlier work.[15] The solvent of the ink was a mixture of 20 wt % Isopropyl alcohol (IPA, Emsure, Merck) and 80 wt % ultrapure water (Milli-Q, Merck). The Pt/V catalyst used in this paper is a 20 wt % Pt on Vulcan carbon support (Tanaka, TEC10V20E) and the Pt/KB catalyst is a 20 wt % Pt on Ketjenblack carbon support (Tanaka, TEC10E20E). The inks were prepared as in the following procedure: First, the catalyst powder was weighed into a roll mill vial, then the solvent was added, and then the ionomer (Nafion D520, Chemours). The amount of the ionomer was adjusted to the Ionomer to Carbon ratio (I/C ratio) of 0.4−1.2. The inks with a fixed solid weight content of 3 wt % were homogenized by roll milling for 18 h. By using an ultrasonic spray coater (SonoTec) with the temperature of the heating stage of 100 °C, shaping air of 0.60 psi, and a flow rate of 0.25 mL min^{-1}, the ink was applied onto Freudenberg H23C8 gas diffusion media. The deposition rate was ∼5−7 μg_{Pt} cm^{-2} per cycle, and the loading was determined by sample weight before and after spray coating (Sartorius Cubis, ±0.001 mg). The final loading of the samples was controlled to 0.1 mg_{Pt} cm^{-1}.

2.2. Electrochemical Half-Cell, Experiments and Cleaning. *2.2.1. GDE.* The design of the gas diffusion electrode half-cell setup used in our group was introduced in a previous publication and can be found again in the Supporting Information.[16,33] The GDE half-cell is made out of PTFE and contains a liquid electrolyte compartment and a gas compartment. The flow field in the gas compartment is a graphite flow field (R8710, SGL CARBON) with an electrical resistance of 13 μΩ. All experiments are performed at room temperature in 1 M $HClO_4$ (70% Emsure, Merck), with a H_2 reference electrode (Gaskatel), and a counter electrode of Ir/Ta mixed metal oxide (METAKEM). A Biologic potentiostat (VMP-300, 2 A booster boards) was used for the electrochemical measurements. The electrochemical protocol, including the electrochemical wetting, electrochemical cleaning, and basic characterization as well as the AST experiments are described in detail in the Supporting Information.

The liquid electrolyte compartment was always stored in ultrapure water (Milli-Q, Merck). Between different I/C ratios and carbon supports tests, the cell was boiled in 1% HNO_3 (70% Emsure, Merck, and ultrapure water, Milli-Q, Merck) and five times in water. Additionally, the cell was again boiled twice in ultrapure water between each of the three replicates of each batch. The used gases Ar (99.998%, Air Liquide), H_2 (99.999%, Air Liquide), O_2 (99.998%, Air Liquide), and CO (99.997%, Air Liquide) were controlled with a mass flow controller (Bronkhorst).

2.2.2. GDE-ICP-MS. The coupling of a GDE half-cell with an ICP−MS was introduced in our previous publication.[15,24] The detailed description of the electrochemical protocol can be found in the Supporting Information. In general, before the GDE-ICP-MS measurement, a calibration of the ICP−MS (PerkinElmer, Nexion 350X) by a four-point calibration (0, 2.5, 5, 25 μg L^{-1}) with a standard Pt solution prepared from Merck Certipur ICP standards (H_2PtCl_6, 1000 mg L^{-1} in 7% HCl) was done daily. An internal standard of ^{187}Re (SigmaAldrich, traceCERT, 1000 mg L^{-1}, in 2%

https://doi.org/10.1021/acsaem.5c00184
ACS Appl. Energy Mater. 2025, 8, 7939−7947

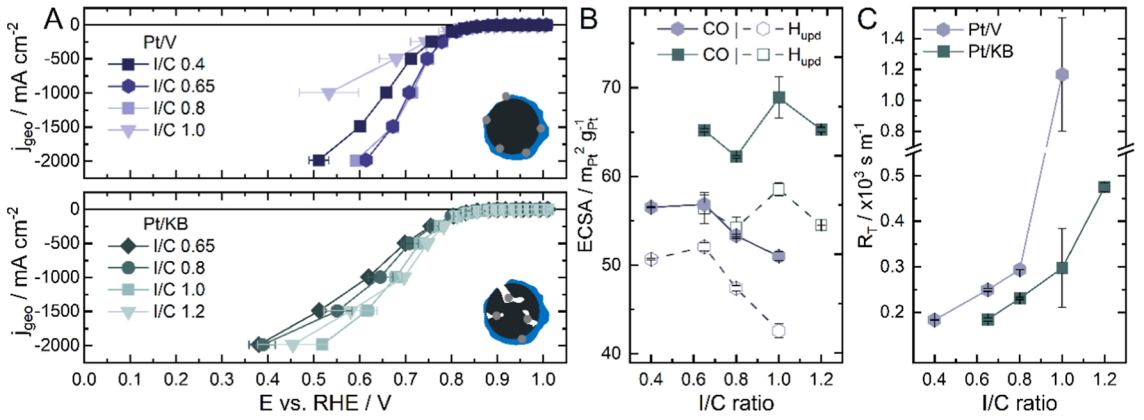

Figure 1. Electrochemical investigation of Pt/V (purple) and Pt/KB (green) with four different I/C ratios each. (A) Performance of Pt/V and Pt/KB for all I/C ratios (Detailed version in the Supporting Information). (B) ECSA of both catalysts determined by CO-stripping and H_{upd} (C) O_2 mass transport resistance, R_T, of limiting current measurements for all I/C ratios.

HNO_3) with a final concentration of 50 μg L^{-1} in 1% HNO_3 was used for all experiments. The flow rate to the ICP−MS was always ∼190 μL min^{-1}. The experiments have been performed in 0.1 M $HClO_4$ (70% Emsure, Merck) to use moderate conditions for the ICP−MS. The setup, including the H_2 reference electrode (Gaskatel), a counter electrode of Ir/Ta mixed metal oxide (METAKEM), and a Biologic potentiostat (VMP-300, 2 A booster boards), was used for all electrochemical measurements. The measurements for the Pt/V I/C 1.0, Pt/V I/C 0.65, and Pt/KB I/C 1.0 were executed three times for each sample.

2.2.3. Scanning Electron Microscopy (SEM). The CLs thickness was determined by analyzing cross-sectional samples. The electrodes have been embedded into epoxy resin (Epo Thin 2, Buehler) and put in a vacuum environment for ∼20 min (air bubble elimination). The samples were dried overnight at room temperature and then ground using an automatic polishing machine (LaboForce-100, Struers GmbH). After grinding the sample with silicon carbide grinding paper (Struers GmbH), the conductivity was improved by gold sputter coating on the samples (108 Manual Sputter Coater, Cressington). The imaging was done by using a Phenom XL (Thermo Fisher) tabletop scanning electron microscope (SEM) with an electron-backscatter detector and 15 kV acceleration to visualize the contrast between carbon and Pt-rich regions (Supporting Information).

3. RESULTS

In GDE half-cell setups, as well as in MEAs, the I/C ratio is one of the most important parameters for optimizing the transport processes within the CL.[11] Since the I/C ratio is adjusted to optimize the triple-phase interface and, therefore, achieve the best performance, it is a crucial parameter for every new catalyst/ionomer system.

The target is to perform dissolution experiments and compare realistic CLs of the two model catalysts Pt/V and Pt/KB in the GDE half-cell. First, a benchmarking study is needed to find the performance-optimized CL, identifying the optimal I/C ratio by analyzing the ECSA (H_{upd} and CO-stripping), performance curves in O_2, and O_2 mass transport resistance (Section 3.1). This is followed by directly comparing the intrinsic properties of the best-performing Pt/V and Pt/KB CLs and a cycling AST of 5000 iterations (Section 3.2). Finally, the analysis of the catalyst stability, focusing on the dissolution of the Pt ions from the CL, was performed (Section 3.3).

3.1. Optimizing the Performance of Pt/V and Pt/KB. When focusing on the two benchmark catalysts, Pt/V and Pt/KB, the literature suggests that the performance-optimized I/C ratio in MEAs ranges from 0.54 to 0.83 for a nonporous support,[7,34,35] whereas for a porous support, such as the Pt/KB, the optimum I/C ratio is around 0.9−1.1.[11] In the GDE literature, for Pt/V with high Pt loading (40 wt % Pt on carbon), an optimized I/C ratio of 0.7[33] has been found; however, no study has yet been conducted to analyze different I/C ratios for Pt/KB for the suggested I/C ratio range.

Identifying the performance-optimized CL for Pt/V, which we expect in a similar range mentioned above for MEAs, the I/C ratios of 0.4, 0.65, 0.8, and 1.0 were tested in this work. For the I/C study of Pt/KB, ratios of 0.65, 0.8, 1.0, and 1.2 were analyzed. The characterization of the different CLs consisted of determining the ECSA via H_{upd} and CO-stripping, performance curves in O_2, and O_2 mass transport resistance (Figure 1). It is important to mention that for CLs with different carbon supports, the manufacturing process, especially the ink composition and activation, plays a crucial role. In comparison to the Pt/V, the Pt/KB needed longer conditioning time until the ECSA stabilized, which is probably related to the wetting of the micropores (Supporting Information). A summary of the activation in GDE, focusing on Pt/V, can be seen in our previous publication, while details of Pt/KB have been added to the Supporting Information.[26]

The Pt/V with an I/C ratio of 0.65 shows the best performance with E = ∼0.6 V at high current densities of 2 A cm^{-2}. Significant losses occur, especially with a meagre I/C ratio of 0.4, as well as with a high I/C ratio of 1.0. In fact, the inaccessibility of the surface seems to be more critical when having a high ionomer content than with a lower ionomer content. This is already reported in GDE half-cell literature for Pt/V, where an increase of the I/C ratio increases the losses at high current densities much more than using a lower content.[33] At high I/C ratios, the macropores are filled, and the thick ionomer layer hinders the oxygen from accessing the active sides of Pt. In contrast, direct contact with the electrolyte and complete wetting of the CL with water ensures proton transport. The I/C ratios of 0.65 and 0.8 exhibit very similar performance, consistent with the I/C ratios found in the literature.[7,34,35] The optimum I/C ratio may be in this range, but this was not pursued further due to the small difference between these two I/C ratios.

The Pt/KB, on the other hand, shows the best performance with an I/C ratio of 1.0, which agrees with the MEA literature of 0.9−1.1 for Pt/KB CLs.[11] Based on the performance curves,

https://doi.org/10.1021/acsaem.5c00184
ACS Appl. Energy Mater. 2025, 8, 7939−7947

significant losses also occur at a low I/C ratio of 0.65, as well as at a high I/C ratio of 1.2, where the same arguments are valid as mentioned above. It should be noted that the I/C ratios observed in this study are specific to the ionomer used and experimental conditions. As in MEA, we would expect different water management for other ionomers or conditions, leading to different optimal I/C ratios. However, this influence needs to be investigated and verified in future work in order to describe the full influence of the I/C ratio in the GDE half-cells.[36,37]

The ECSA was evaluated via the H_{upd} area of CVs and with CO-stripping. The GDE half-cell literature already describes that there may be differences between the two methods depending on the analysis method or evaluation as an underestimation of the ECSA via H_{upd} when compared with CO-stripping.[16,38] The inaccuracy is attributed to the lower potential limit (LPL) for the CV profiles where the hydrogen evolution reaction starts and causes an underestimation of the ECSA of the H_{upd} value.[16,19,38] These differences can also be seen in the results exhibited in this study (Figure 1B), whereby the evaluation using H_{upd} shows 9−17% less ECSA than the determined using CO-stripping. The correlation of the ECSA on the I/C ratio is independent of the method chosen, H_{upd} or CO-stripping, and shows similar behavior for Pt/V and Pt/KB. Both illustrate a relatively constant ECSA over the entire I/C range, with a maximum ECSA deviation of 7 to 10%. This trend aligns with the literature on other I/C studies with GDE on Pt/V with a high Pt content, showing only small deviations within the I/C ratios.[33]

Comparing the ECSAs of the two different supports, Pt/V and Pt/KB, in the GDE half-cell setup (Figure 1B), the Pt/KB exhibits a constant higher ECSA than Pt/V for every I/C ratio. In the MEA literature, the difference in ECSA for different supports can be determined in dry and wet conditions. For dry conditions, the ECSA values for Pt/V and Pt/KB vary significantly. As catalysts with Vulcan supports have most of the Pt NPs on the outer surface of the carbon support, all the Pt NPs are accessible under dry conditions. Porous supports, such as Ketjenblack, exhibit lower ECSA under dry conditions as they do not only have the Pt NPs at the exterior but also a fraction of the NPs are embedded inside the pores, and the water pathways in the porous carbon structure are diminished—leading to a loss of measured ECSA.[12,33] By measuring at high relative humidities (i.e., RH = 80%), the extreme difference in ECSA values is no longer noticeable as at humidified conditions, the Pt NPs inside the pores are also accessible.[12,33] GDE half-cell setups are assumed to be fully wetted systems because the CLs are directly exposed to the liquid electrolyte. Thus, the differences in the ECSA between the samples of Pt/V and Pt/KB CLs shown in this study are comparable to those observed at high relative humidities in the MEA results.

The O_2 mass transport resistance, R_T, was determined using the limiting current method, which our group recently introduced in an I/C ratio study on a Pt/V catalyst with high 40 wt % Pt/C.[33] The behavior of the Pt/V catalyst with 20 wt % Pt is similar to that described in the literature for 40 wt % Pt.[33] The higher the I/C ratio, the higher the R_T. After reaching an optimal I/C ratio (Pt/V: I/C 0.65 and Pt/KB I/C 1.0), a significant increase in the oxygen mass transport resistance is observed, which indicates an increase in the ionomer layer thickness and less microporosity of the CL. The R_T for Pt/KB also increases with a higher I/C ratio, whereas the absolute value of the O_2 resistance is higher for Pt/V for the same ionomer content. As a thin homogeneous ionomer layer can be assumed on the carbon support due to the ultrasonic spray coating, the layer thickness of the ionomer on the surface correlates with the size and composition of the carbon. This is often correlated to the BET surface of the carbon support. The Vulcan support has a low surface area (164.1 $m^2\ g^{-1}$, according to the manufacturer), and the ionomer layer has only a limited area to be dispersed on the surface. Thus, an increase in the ionomer layer is expected in the range of I/C 0.65−0.8. The Ketjenblack support has a higher surface area (546.2 $m^2\ g^{-1}$, according to the manufacturer), which results in a lower ionomer layer thickness for the same I/C ratio. Interestingly, focusing on the performance-optimized CLs, Pt/V I/C 0.65, and Pt/KB I/C 1.0, the O_2 mass transport resistances of $R_{T,Pt/V}$ = 249.4 s m^{-1} and $R_{T,Pt/KB}$ = 297.4 s m^{-1} are relatively comparable, indicating a similar ionomer thickness on the Pt NPs in both cases. The results demonstrated a comprehensive characterization using a GDE half-cell setup by applying electrochemical techniques to different catalysts differentiated by carbon supports. Nevertheless, it must be stated that the general tendency is in contrast to the outcomes observed in the MEA. In the MEA, mass transport losses for Pt/KB are higher than for Pt/V at full humidifaction. As the mass transport resistance is a function of the length, width, and tortuosity of the pore diffusion path for O_2 to the Pt particles,[32] it is not entirely possible to exclude the probability of differing humidification of the two CLs in the GDE half-cell at this point. Particularly, the increased hydrophobicity of Pt/KB can have a significant impact on the water management within the CL itself, implying that varying humidification of the CL cannot be entirely dismissed and necessitates further investigation. Especially this different behavior of the water management could also explain the different polarization curves, which despite lower mass transport resistance, show a decreased performance at high current densities for the Pt/KB.

Crucial data regarding Pt/V and Pt/KB CLs with different ionomer content was evaluated and showed similar performance-optimized CLs for Pt/V with an I/C 0.65 and Pt/KB with an I/C 1.0 as in MEA.[11,39] To gain further insight into the behavior of the CLs at the beginning of life (BOL) and end of life (EOL) when utilizing various carbon supports, the next section will focus on the comparison of the optimized CLs for Vulcan and Ketjenblack catalyst layers.

3.2. Comparison of Performance-optimized Pt/V and Pt/KB. The benchmarking results from Section 3.1 clearly distinguish between the optimal I/C ratios of Pt/V and Pt/KB. A direct comparison and indication of the durability of the performance-optimized CLs are obtained by using an AST consisting of 5000 potential cycles (Figure 2).

In both, the low current region (Figure 2, inset) and the high current region, the Pt/V shows similar or better performance than Pt/KB. The potential between the curves up to 500 mA cm^{-2} overlaps completely, indicating a similar activity of both catalysts. Additionally, the Tafel slopes for Pt/V of 54 mV dec^{-1} and for Pt/KB of 54 mV dec^{-1} confirm the identical ORR mechanism and absence of mass transport limitations for the two CLs. However, focusing on the high current densities, the difference at 2 A cm^{-2} of approximately 100 mV indicates higher mass transport losses for the Pt/KB. This demonstrates similar behavior in the high current density region as in MEA, as the oxygen transport to the Pt NPs in the

https://doi.org/10.1021/acsaem.5c00184
ACS Appl. Energy Mater. 2025, 8, 7939−7947

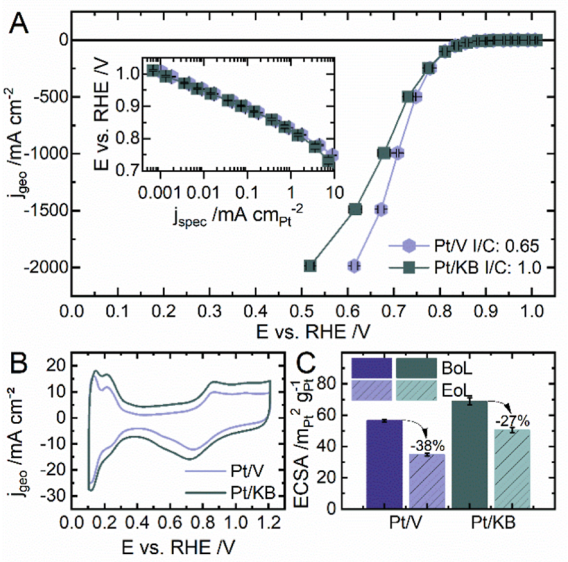

Figure 2. Comparison of the performance-optimized CL of Pt/V with an I/C ratio of 0.65 and Pt/KB with an I/C ratio of 1.0. (A) Performance of the CLs. (B) CVs. (C) ECSA: BOL and EOL (after 5000 CVs in a potential window of 0.1−1.2 V vs RHE at RT).

pores is not as facile as to the Pt NPs on the exterior of the Vulcan.[12,40,41] Other works of RDE and MEA show higher activity for Pt/KB, suggesting less contact of the ionomer with the particles in the pores of the Ketjenblack and resulting in lower poisoning due to the sulfur of the ionomer.[32,42,43] Using similar catalysts, Kobayashi et al., studied the performance of these CLs in MEA, exhibiting little differences at lower current densities. When using carbon supports with other structures of the pores, the intrinsic activity of the catalyst could be enhanced much more than that of Pt/V and Pt/KB.[11] As this is not the case for the results shown in this paper, further studies are needed on the possible influence of the 1 M $HClO_4$ in the GDE half-cell setup on the intrinsic properties of the Pt/C CL, similar to what was recently shown for IrO_x catalyst layer during the oxygen evolution reaction (OER).[44,45] Additionally, as the activity includes the efficient proton supply in the Pt particles' microenvironment, a different proton delivery due to slight differences in humidity resulting from the intrinsic properties of the catalyst, or the configuration in the GDE half-cell setup, could be a potentially reason for the missing differences in activity Pt/V and Pt/KB. Therefore, further study is needed to thoroughly understand these environments, CL and setup specific, and their effects on the catalyst's activity.

The CVs of the optimized CLs exhibit similar features for the oxide and H_{upd} regions (Figure 2B). Differences are mainly in the double-layer capacitance C_{dl} of the two CLs, which depends on the BET surface area of the carbon support for each catalyst. As mentioned in Section 3.1, Pt/V has a lower BET surface area as Pt/KB, in alignment with the C_{dl} results obtained from Figure 2B where the calculated value of Pt/KB ($C_{dl,\ Pt/KB}$ = 58.9 mF cm^{-2}) is about 54% higher than for Pt/V ($C_{dl,\ Pt/V}$ = 27.0 mF cm^{-2}). A similar trend for Pt/V compared to a Pt/HSA carbon (high surface area carbon) is shown in MEA, as the Pt/HAS carbon shows 23% higher C_{dl} as the Pt/V at fully humidified conditions.[46]

The BOL ECSA (CO-stripping) of the Pt/KB CL is 67.1 ± 0.6 $m^2_{Pt}\ g^{-1}_{Pt}$, whereas for the Pt/V CL is 56.5 ± 0.7 $m^2_{Pt}\ g^{-1}_{Pt}$, both in agreement with the literature.[11,40,47] A study on an AST by potential cycling between 0.1 and 1.2 V versus RHE at room temperature (RT) for 5000 cycles indicated higher stability for the Pt/KB than for the Pt/V. The ECSA loss after cycling AST of 0.1−1.2 V vs RHE for the Pt/V CLs in GDE half-cell is ∼40%, and for the Pt/KB is ∼30%. Literature on Pt/V for potential cycling in RDE shows a similar ECSA loss of ∼45% after 5000 cycles as in our experiments.[48] Recent literature showcases similar catalysts (TKK 20 wt % Pt on V and KB) in MEA at 80 °C using square-wave based voltage cycles between 0.6 and 1.0 V, with a hold time of 1 s at each. The results highlight that Pt/V and Pt/KB have a similar slope of a linearly approximated ECSA degradation rate; however, they are steeper for Vulcan,[32] which confirms our trend of ECSA loss found in the GDE half-cell.

To summarize, the results of the GDE half-cell present an intermediate phase between fundamental and applied research. In particular, the good correlation with the trends in MEA shows promising possibilities. Nevertheless, it must be emphasized that quantifying ORR activity, in particular, requires further investigation. In addition, the AST results of 27% and 38% ECSA loss after the 5000 cycles also show potential for longer and more dedicated ASTs, which not only further highlights the differences between the two catalysts, but also opens the way for other post-analysis techniques as the differences are more significant. Still, identifying degradation mechanisms that lead to the different ECSA losses for Pt/V and Pt/KB needs to be investigated—which will be focused on in the next section.

3.3. Dissolution Behavior of Pt on Different Supports and Classification of the Effects Concerning Catalyst Layer Thickness. Various degradation mechanisms are discussed in the literature, including Ostwald ripening, detachment (or electrochemical disconnection), and dissolution (loss of Pt into the bulk electrolyte or ionomer/membrane).[27] To describe the degradation mechanism of the performance-optimized CLs for Pt/V and Pt/KB, one of the key factors is the dissolution behavior of Pt^{2+} ions. Here, we need to distinguish between the dissolution behavior in the vicinity of the Pt particle where redeposition could take place, which is called Ostwald ripening, and the escaping of Pt^{2+} ions out of the CL, which is then called dissolution. The differences between Ostwald ripening and dissolution in real CLs have not yet been fully clarified, especially when focusing on the difference between Pt/V and Pt/KB and the interplay with ionomer. In MEA, the dissolution can be characterized by post-mortem characterization visualizing the Pt band in the membrane after an AST.[30,49] Ostwald ripening can be illustrated by post-mortem analysis of the CL by determining the particle size increase, often confirmed by TEM images.[49]

However, since the differences between the two catalysts have only been investigated ex-situ in MEAs, focusing mainly on the qualitative investigation of the Pt-band formation and the particle size, an in situ method is still missing to analyze the differences between Pt/V and Pt/KB quantitatively. One approach to overcome this is to use online characterization with the GDE-ICP-MS method to clarify the differences in the dissolution of real CLs of Vulcan and Ketjenblack. The protocol used is similar to previous studies for GDE-ICP-MS measurements,[24] starting with two slow CVs to determine the BOL with a scan rate of 10 mV s^{-1} ranging from 0.1 to 1.5 V. The next step was to perform a short AST using 200 CVs with 200 mV s^{-1} ranging from 0.1 to 1.5 V. The EOL

https://doi.org/10.1021/acsaem.5c00184
ACS Appl. Energy Mater. 2025, 8, 7939−7947

characterization was determined by two slow CVs of 10 mV s^{-1} in a range from 0.1 to 1.5 V.

The study of time-resolved potential and dissolution profile for the different CLs focuses on the performance-optimized CLs of Section 3.2. The faster degradation (ECSA-loss) for Pt/V may be caused by both degradation mechanisms, Ostwald ripening and dissolution.[32] As some of the Pt particles are in the pores of the Pt/KB, the chance that the Pt ions redeposit back on the source Pt particles, due to a longer escape path, should be higher—resulting in lower apparent dissolution of the detected by ICP–MS Pt^{2+}. Interestingly, both carbon supports show the same trend of detected Pt^{2+}, independent from the applied potential. No significant differences can be detected either in the BOL CVs nor in the AST or EOL characterization. Especially with an increased redeposition rate for the Pt/KB, there should be a difference during the AST or the EOL characterization.

Another parameter whose influence is still discussed in the literature is the ability of the ionomer to capture the dissolved M^{x+} ions.[45,50] It is possible that the ionomer captures the positively charged M^{x+} ions with the negatively charged SO_3^- groups. To exclude the effect of a possible restraining of the Pt^{x+} in the ionomer and underestimation of the dissolution of Pt/KB with a performance-optimized I/C ratio of 1.0, a Pt/V CL with an I/C ratio of 1.0 was also investigated. The results for the Pt/V with an I/C ratio of 1.0 present similar dissolution profiles, as well as integrated findings for the performance-optimized catalyst layers of Pt/V and Pt/KB (Figure 3). The integrated peaks of the BOL, AST, and EOL confirm the qualitative observation of the dissolution profiles (Figure 3B). All three CLs show similar dissolution within the error bars, indicating negligible differences in dissolution of the different carbon supports.

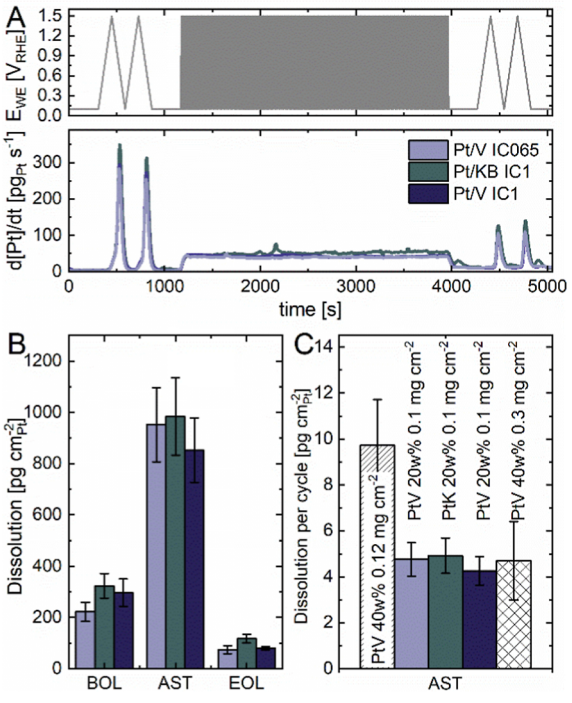

Figure 3. Pt dissolution results for Pt/KB with an I/C ratio of 1.0 (performance-optimized) and Pt/V with I/C ratios of 0.65 (performance-optimized) and 1.0 (similar to performance-optimized I/C ratio of Pt/KB) obtained in GDE-ICP-MS in 0.1 M $HClO_4$. (A) The time-resolved protocol of applied potential (top) and the dissolution (bottom). (B) Summary of the dissolution results for BOL, AST, and EOL normalized by specific area of the Pt. (C) Comparison of the obtained result with dissolution results of different CLs thicknesses, compared to dissolution studies from the literature.[24]

It seems that the determining factor for the dissolution out of real CLs is mainly the electrode thickness and not the carbon support/ionomer content in the first place. In the literature,[24] Pt/V with 40 wt % Pt with loadings of 0.12 mg cm^{-2} and 0.3 mg cm^{-2} were used, and an electrode thickness of ∼5 and ∼11 μm for these CLs can be estimated (Figure 3C and Supporting Information).[15,24] The results of the performance-optimized CLs thicknesses in this study are 9.73 ± 0.47 μm for Pt/V and 12.88 ± 0.76 μm for Pt/KB (Supporting Information). The CLs with a thickness of ∼11 μm have a dissolution per cycle of ∼4 pg cm^{-2}_{Pt}. In contrast, the CL with a loading of 0.12 mg cm^{-2} of the Pt/V 40 w % Pt (and an I/C ratio of 0.7) and an electrode thickness of ∼5 μm shows a dissolution per cycle of ∼10 pg cm^{-2}_{Pt} resulting in a factor of 2 compared to the results of the different carbons (Figure 3C).

The results indicate that the differences in the dissolution, described as Pt^{2+} ions diffusion out of the CL, of a Vulcan and Ketjenblack support are negligible. Consequently, we conclude that the main degradations in the ECSA loss are due to Ostwald ripening or electrochemical disconnection (supported by the STEM images in the Supporting Information). We would like to stress, however, that this conclusion is based on the results obtained using the chosen AST protocols. Additionally, as mentioned in Section 3.2, longer ASTs would not only stress the different degradation of Vulcan and Ketjenblack, it would also open the way for further analytical methods such as thickness measurement of the degraded CLs to fully exclude the presence of carbon corrosion. In the future, an experimental approach should be used to study how parameters of AST (e.g., potential range and electrolyte temperature) influence the degradation mechanism of Pt with different carbon supports.

4. CONCLUSION AND OUTLOOK

This work presents a novel approach to investigate Pt catalyst for PEMFC application with different carbon supports, namely Vulcan as a nonporous representative and Ketjenblack as a porous representative. The electrochemical measurements performed in the GDE half-cell setup align in the majority of the results with MEA literature and show a good correlation between the trends described for Pt/V and Pt/KB. The possibility of determining the optimal I/C ratio for Pt/V of 0.65 and Pt/KB with 1.0 has opened the way for an appropriate investigation with the GDE half-cell setup. A comparison of the optimized CLs for Pt/V and Pt/KB shows a better BOL performance for the Pt/V as mass transport losses for the Pt/KB dominate in the high current density region. A cycling AST between 0.1 and 1.2 V for 5000 cycles exhibits a decrease in ECSA for Pt/V of ∼40% and for Pt/KB of ∼30%, indicating better stability for the Pt/KB CL. Using the GDE-ICP-MS setup, a fundamental understanding of the degradation mechanism in PEMFC CLs and quantifying the dissolution of the Pt, described by the escaping metal ions out of the CL was performed to distinguish between Ostwald ripening and dissolution. The results do not show a significant influence of the carbon support in the dissolution of Pt under these conditions, identifying Ostwald ripening as the dominating degradation process which is most probably

https://doi.org/10.1021/acsaem.5c00184
ACS Appl. Energy Mater. 2025, 8, 7939−7947

hindered in Pt/KB. The Pt/V I/C 1.0 exhibits similar results as with a lower I/C ratio of 0.65; hence, also a significant influence of the higher I/C than the performance-optimized CLs can be excluded, and the possible interference of different properties can be ruled out. These results present the importance of the catalyst design and, specifically, the prevention of the Ostwald ripening process in new catalyst designs for PEMFC. Nevertheless, further fundamental studies are required, such as the investigation of the different supports for the protocols used here, focusing on the operating range and temperature of fuel cells,[51] and a complete understanding of the degradation mechanisms.

■ ASSOCIATED CONTENT

Supporting Information

The Supporting Information is available free of charge at https://pubs.acs.org/doi/10.1021/acsaem.5c00184.

Extrapolation of CL thickness from ref, design of the GDE half-cell, electrochemical protocols, electrochemical cleaning, determination of CL thickness, TEM images (PDF)

■ AUTHOR INFORMATION

Corresponding Authors

Pascal Lauf − *Helmholtz-Institute Erlangen-Nürnberg for Renewable Energy (IET-2), Forschungszentrum Jülich GmbH, 91058 Erlangen, Germany; Department of Chemical and Biological Engineering, Friedrich-Alexander University Erlangen-Nürnberg, 91058 Erlangen, Germany;* orcid.org/0000-0002-8438-8238; Email: p.lauf@fz-juelich.de

Serhiy Cherevko − *Helmholtz-Institute Erlangen-Nürnberg for Renewable Energy (IET-2), Forschungszentrum Jülich GmbH, 91058 Erlangen, Germany;* orcid.org/0000-0002-7188-4857; Email: s.cherevko@fz-juelich.de

Authors

A. Lucía Morales − *Helmholtz-Institute Erlangen-Nürnberg for Renewable Energy (IET-2), Forschungszentrum Jülich GmbH, 91058 Erlangen, Germany; Department of Chemical and Biological Engineering, Friedrich-Alexander University Erlangen-Nürnberg, 91058 Erlangen, Germany*

Konrad Ehelebe − *Helmholtz-Institute Erlangen-Nürnberg for Renewable Energy (IET-2), Forschungszentrum Jülich GmbH, 91058 Erlangen, Germany; Department of Chemical and Biological Engineering, Friedrich-Alexander University Erlangen-Nürnberg, 91058 Erlangen, Germany;* orcid.org/0000-0001-9441-5642

Andreas Hutzler − *Helmholtz-Institute Erlangen-Nürnberg for Renewable Energy (IET-2), Forschungszentrum Jülich GmbH, 91058 Erlangen, Germany;* orcid.org/0000-0001-5484-707X

Karl J. J. Mayrhofer − *Helmholtz-Institute Erlangen-Nürnberg for Renewable Energy (IET-2), Forschungszentrum Jülich GmbH, 91058 Erlangen, Germany; Department of Chemical and Biological Engineering, Friedrich-Alexander University Erlangen-Nürnberg, 91058 Erlangen, Germany;* orcid.org/0000-0002-4248-0431

Vicent Lloret − *Helmholtz-Institute Erlangen-Nürnberg for Renewable Energy (IET-2), Forschungszentrum Jülich GmbH, 91058 Erlangen, Germany*

Complete contact information is available at: https://pubs.acs.org/10.1021/acsaem.5c00184

Author Contributions

P.L. and S.C. conceived and planned the experiments. P.L. and A.L.M. carried out the experiments. P.L. and A.L.M. analyzed and summarized the data. P.L., A.L.M., K.E., V.L., K.J.J.M. & S.C. contributed to the interpretation of the results. A.H. provided the TEM images. P.L. took the lead in writing the manuscript. All authors provided critical feedback and helped shape the research, analysis and manuscript.

Notes

The authors declare no competing financial interest.

■ ACKNOWLEDGMENTS

P.L., K.E., V.L., K.J.J.M. and S.C. acknowledge funding by the German Federal Ministry for Economic Affairs and Energy (BMWi) within the POREForm project (03ETB027A). K.E. acknowledges Heinrich Böll Foundation for financial support. P.L. wants to thank Andreas Körner for supporting the TEM measurements and discussions.

■ REFERENCES

(1) Rhodes, C. J. The 2015 Paris Climate Change Conference: Cop21. *Sci. Prog.* **2016**, *99* (1), 97−104.

(2) Bernhart, W.; Riederle, S.; Yoon, M.; Aulbur, W. G. Fuel Cells — A Realistic Alternative for Zero Emission? *Auto Tech Rev.* **2014**, *3* (3), 18−23.

(3) Olabi, A. G.; Wilberforce, T.; Abdelkareem, M. A. Fuel Cell Application in the Automotive Industry and Future Perspective. *Energy* **2021**, *214*, 118955.

(4) Stacy, J.; Regmi, Y. N.; Leonard, B.; Fan, M. The Recent Progress and Future of Oxygen Reduction Reaction Catalysis: A Review. *Renewable Sustainable Energy Rev.* **2017**, *69*, 401−414.

(5) Ly, A.; Asset, T.; Atanassov, P. Integrating Nanostructured Pt-Based Electrocatalysts in Proton Exchange Membrane Fuel Cells. *J. Power Sources* **2020**, *478*, 228516.

(6) Owejan, J. P.; Owejan, J. E.; Gu, W. Impact of Platinum Loading and Catalyst Layer Structure on PEMFC Performance. *J. Electrochem. Soc.* **2013**, *160*, F824.

(7) Antolini, E.; Giorgi, L.; Pozio, A.; Passalacqua, E. Influence of Nafion Loading in the Catalyst Layer of Gas-Diffusion Electrodes for PEFC. *J. Power Sources* **1999**, *77* (2), 136−142.

(8) Kim, K.-H.; Lee, K.-Y.; Kim, H.-J.; Cho, E.; Lee, S.-Y.; Lim, T.-H.; Yoon, S. P.; Hwang, I. C.; Jang, J. H. The Effects of Nafion® Ionomer Content in PEMFC MEAs Prepared by a Catalyst-Coated Membrane (CCM) Spraying Method. *Int. J. Hydrogen Energy* **2010**, *35* (5), 2119−2126.

(9) Sasikumar, G.; Ihm, J. W.; Ryu, H. Dependence of Optimum Nafion Content in Catalyst Layer on Platinum Loading. *J. Power Sources* **2004**, *132* (1), 11−17.

(10) Perez-Alonso, F. J.; McCarthy, D. N.; Nierhoff, A.; Hernandez-Fernandez, P.; Strebel, C.; Stephens, I. E. L.; Nielsen, J. H.; Chorkendorff, I. The Effect of Size on the Oxygen Electroreduction Activity of Mass-Selected Platinum Nanoparticles. *Angew. Chem., Int. Ed.* **2012**, *51* (19), 4641−4643.

(11) Kobayashi, A.; Fujii, T.; Harada, C.; Yasumoto, E.; Takeda, K.; Kakinuma, K.; Uchida, M. Effect of Pt and Ionomer Distribution on Polymer Electrolyte Fuel Cell Performance and Durability. *ACS Appl. Energy Mater.* **2021**, *4* (3), 2307−2317.

(12) Yarlagadda, V.; Carpenter, M. K.; Moylan, T. E.; Kukreja, R. S.; Koestner, R.; Gu, W.; Thompson, L.; Kongkanand, A. Boosting Fuel Cell Performance with Accessible Carbon Mesopores. *ACS Energy Lett.* **2018**, *3* (3), 618−621.

(13) Yu, X.; Ye, S. Recent Advances in Activity and Durability Enhancement of Pt/C Catalytic Cathode in PEMFC: Part I. Physico-chemical and electronic Interaction between Pt and Carbon Support,

and Activity Enhancement of Pt/C Catalyst. *J. Power Sources* **2007**, *172* (1), 133−144.
(14) Ehelebe, K.; Escalera-López, D.; Cherevko, S. Limitations of Aqueous Model Systems in the Stability Assessment of Electrocatalysts for Oxygen Reactions in Fuel Cell and Electrolyzers. *Curr. Opin. Electrochem.* **2021**, *29*, 100832.
(15) Ehelebe, K.; Seeberger, D.; Paul, M. T. Y.; Thiele, S.; Mayrhofer, K. J. J.; Cherevko, S. Evaluating Electrocatalysts at Relevant Currents in a Half-Cell: The Impact of Pt Loading on Oxygen Reduction Reaction. *J. Electrochem. Soc.* **2019**, *166* (16), F1259−F1268.
(16) Ehelebe, K.; Schmitt, N.; Sievers, G.; Jensen, A. W.; Hrnjić, A.; Collantes Jiménez, P.; Kaiser, P.; Geuß, M.; Ku, Y.-P.; Jovanovič, P.; Mayrhofer, K. J. J.; Etzold, B.; Hodnik, N.; Escudero-Escribano, M.; Arenz, M.; Cherevko, S. Benchmarking Fuel Cell Electrocatalysts Using Gas Diffusion Electrodes: Inter-lab Comparison and Best Practices. *ACS Energy Lett.* **2022**, *7* (2), 816−826.
(17) Pinaud, B. A.; Bonakdarpour, A.; Daniel, L.; Sharman, J.; Wilkinson, D. P. Key Considerations for High Current Fuel Cell Catalyst Testing in an Electrochemical Half-Cell. *J. Electrochem. Soc.* **2017**, *164* (4), F321−F327.
(18) Inaba, M.; Jensen, A. W.; Sievers, G. W.; Escudero-Escribano, M.; Zana, A.; Arenz, M. Benchmarking High Surface Area Electrocatalysts in a Gas Diffusion Electrode: Measurement of Oxygen Reduction Activities under Realistic Conditions. *Energy Environ. Sci.* **2018**, *11* (4), 988−994.
(19) Schmitt, N.; Schmidt, M.; Hübner, G.; Etzold, B. J. M. Oxygen Reduction Reaction Measurements on Platinum Electrocatalysts in Gas Diffusion Electrode Half-Cells: Influence of Electrode Preparation, Measurement Protocols and common Pitfalls. *J. Power Sources* **2022**, *539*, 231530.
(20) Schmitt, N.; Schmidt, M.; Mueller, J. E.; Schmidt, L.; Trabold, M.; Jeschonek, K.; Etzold, B. J. M. Which Insights can Gas Diffusion Electrode Half-Cell Experiments give into Activity Trends and Transport Phenomena of Membrane Electrode Assemblies? *Energy Adv.* **2023**, *2* (6), 854−863.
(21) Loukrakpam, R.; Gomes, B. F.; Prokop, M.; Bauer, C.; Kutter, M.; Baier, F.; Kempe, R.; Roth, C. Challenges and Limitations of Accelerated Stress Testing in GDE Half-Cell Set-Ups. *J. Power Sources* **2023**, *569*, 232905.
(22) Kasuk, K.-A.; Nerut, J.; Grozovski, V.; Lust, E.; Kucernak, A. Design and Impact: Navigating the Electrochemical Characterization Methods for Supported Catalysts. *ACS Catal.* **2024**, *14* (16), 11949−11966.
(23) Hrnjić, A.; Ruiz-Zepeda, F.; Gaberšček, M.; Bele, M.; Suhadolnik, L.; Hodnik, N.; Jovanovič, P. Modified Floating Electrode Apparatus for Advanced Characterization of Oxygen Reduction Reaction Electrocatalysts. *J. Electrochem. Soc.* **2020**, *167* (16), 166501.
(24) Ehelebe, K.; Knoppel, J.; Bierling, M.; Mayerhofer, B.; Bohm, T.; Kulyk, N.; Thiele, S.; Mayrhofer, K. J. J.; Cherevko, S. Platinum Dissolution in Realistic Fuel Cell Catalyst Layers. *Angew. Chem., Int. Ed.* **2021**, *60* (16), 8882−8888.
(25) Delikaya, O.··.; Bevilacqua, N.; Eifert, L.; Kunz, U.; Zeis, R.; Roth, C. Porous Electrospun Carbon Nanofibers Network as an Integrated Electrode@Gas Diffusion Layer for High Temperature Polymer Electrolyte Membrane Fuel Cells. *Electrochim. Acta* **2020**, *345*, 136192.
(26) Lauf, P.; Morales, A. L.; Nozadze, A.; Ayoub, M.; Bierling, M.; Ehelebe, K.; Thiele, S.; Mayrhofer, K. J. J.; Lloret, V.; Cherevko, S. Be Aware of the Effect of Electrode Activation and Morphology on its Performance in Gas Diffusion Electrode Setups. *J. Power Sources* **2024**, *623*, 235352.
(27) Meier, J. C.; Galeano, C.; Katsounaros, I.; Witte, J.; Bongard, H. J.; Topalov, A. A.; Baldizzone, C.; Mezzavilla, S.; Schüth, F.; Mayrhofer, K. J. J. Design Criteria for Stable Pt/C Fuel Cell Catalysts. *Beilstein J. Nanotechnol.* **2014**, *5*, 44−67.
(28) Cherevko, S.; Kulyk, N.; Mayrhofer, K. J. J. Durability of Platinum-Based Fuel Cell Electrocatalysts: Dissolution of Bulk and Nanoscale Platinum. *Nano Energy* **2016**, *29*, 275−298.
(29) Dubau, L.; Castanheira, L.; Maillard, F.; Chatenet, M.; Lottin, O.; Maranzana, G.; Dillet, J.; Lamibrac, A.; Perrin, J.-C.; Moukheiber, E.; ElKaddouri, A.; De Moor, G.; Bas, C.; Flandin, L.; Caqué, N. A Review of PEM Fuel Cell Durability: Materials Degradation, Local Heterogeneities of Aging and Possible Mitigation Strategies. *WIREs Energy Environ* **2014**, *3* (6), 540−560.
(30) Della Bella, R. K. F.; Stühmeier, B. M.; Gasteiger, H. A. Universal Correlation between Cathode Roughness Factor and H2/Air Performance Losses in Voltage Cycling-Based Accelerated Stress Tests. *J. Electrochem. Soc.* **2022**, *169* (4), 044528.
(31) Reichmann, I.; Lloret, V.; Ehelebe, K.; Lauf, P.; Jenewein, K.; Mayrhofer, K. J. J.; Cherevko, S. Scanning Gas Diffusion Electrode Setup for Real-Time Analysis of Catalyst Layers. *ACS Meas. Sci. Au* **2024**, *4*, 515−527.
(32) Lazaridis, T.; Della Bella, R. K. F.; Gasteiger, H. A. Trading Off Initial PEM Fuel Cell Performance versus Voltage Cycling Durability for Different Carbon Support Morphologies. *J. Electrochem. Soc.* **2024**, *171* (6), 064506.
(33) Lauf, P.; Lloret, V.; Geuß, M.; Collados, C. C.; Thommes, M.; Mayrhofer, K. J. J.; Ehelebe, K.; Cherevko, S. Characterization of Oxygen and Ion Mass Transport Resistance in Fuel Cell Catalyst Layers in Gas Diffusion Electrode Setups. *J. Electrochem. Soc.* **2023**, *170* (6), 064509.
(34) Passalacqua, E.; Lufrano, F.; Squadrito, G.; Patti, A.; Giorgi, L. Nafion Content in the Catalyst Layer of Polymer Electrolyte Fuel Cells: Effects on Structure and Performance. *Electrochim. Acta* **2001**, *46* (6), 799−805.
(35) Qi, Z.; Kaufman, A. Low Pt Loading High Performance Cathodes for PEM Fuel Cells. *J. Power Sources* **2003**, *113* (1), 37−43.
(36) Braaten, J. P.; Kariuki, N. N.; Myers, D. J.; Blackburn, S.; Brown, G.; Park, A.; Litster, S. Integration of a high oxygen permeability ionomer into polymer electrolyte membrane fuel cell cathodes for high efficiency and power density. *J. Power Sources* **2022**, *522*, 230821.
(37) Chowdhury, A.; Bird, A.; Liu, J.; Zenyuk, I. V.; Kusoglu, A.; Radke, C. J.; Weber, A. Z. Linking Perfluorosulfonic Acid Ionomer Chemistry and High-Current Density Performance in Fuel-Cell Electrodes. *ACS Appl. Energy Mater.* **2021**, *13* (36), 42579−42589.
(38) Röttcher, N. C.; Ku, Y.-P.; Minichova, M.; Ehelebe, K.; Cherevko, S. Comparison of methods to determine electrocatalysts' surface area in gas diffusion electrode setups: a case study on Pt/C and PtRu/C. *JPhys Energy* **2023**, *5* (2), 024007.
(39) Liu, Y.; Murphy, M. W.; Baker, D. R.; Gu, W.; Ji, C.; Jacob, J.; Gasteiger, H. A. Proton Conduction and Oxygen Reduction Kinetics in PEM Fuel Cell Cathodes: Effects of Ionomer-to-Carbon Ratio and Relative Humidity. *J. Electrochem. Soc.* **2009**, *156* (8), 12.
(40) Padgett, E.; Yarlagadda, V.; Holtz, M. E.; Ko, M.; Levin, B. D. A.; Kukreja, R. S.; Ziegelbauer, J. M.; Andrews, R. N.; Ilavsky, J.; Kongkanand, A.; Muller, D. A. Mitigation of PEM Fuel Cell Catalyst Degradation with Porous Carbon Supports. *J. Electrochem. Soc.* **2019**, *166* (4), F198−F207.
(41) Qi, Y.; Huang, Y.; Gao, Z.; Chen, C. H.; Perego, A.; Yildirim, H.; Odgaard, M.; Asset, T.; Atanassov, P.; Zenyuk, I. V. Insight into carbon corrosion of different carbon supports for Pt-based electrocatalysts using accelerated stress tests in polymer electrolyte fuel cells. *J. Power Sources* **2022**, *551*, 232209.
(42) Shinozaki, K.; Morimoto, Y.; Pivovar, B. S.; Kocha, S. S. Suppression of Oxygen Reduction Reaction Activity on Pt-Based Electrocatalysts from Ionomer Incorporation. *J. Power Sources* **2016**, *325*, 745−751.
(43) Zeng, J.; Jean, D.-i.; Ji, C.; Zou, S. In Situ Surface-Enhanced Raman Spectroscopic Studies of Nafion Adsorption on Au and Pt Electrodes. *Langmuir* **2012**, *28* (1), 957−964.
(44) Geuß, M.; Milosevic, M.; Bierling, M.; Löttert, L.; Abbas, D.; Escalera-López, D.; Lloret, V.; Ehelebe, K.; Mayrhofer, K. J. J.; Thiele, S.; Cherevko, S. Investigation of Iridium-Based OER Catalyst Layers in a GDE Half-Cell Setup: Opportunities and Challenges. *J. Electrochem. Soc.* **2023**, *170* (11), 114510.

https://doi.org/10.1021/acsaem.5c00184
ACS Appl. Energy Mater. 2025, 8, 7939−7947

(45) Geuß, M.; Löttert, L.; Böhm, T.; Hutzler, A.; Mayrhofer, K. J. J.; Thiele, S.; Cherevko, S. Quantification of Iridium Dissolution at Water Electrolysis Relevant Conditions Using a Gas Diffusion Electrode Half-Cell Setup. *ACS Catal.* **2024**, *14* (15), 11819−11831.
(46) Qi, Y.; Morimoto, Y.; Shibata, M. S.; Gao, Z.; Sabarirajan, D. C.; Haug, A. T.; Zenyuk, I. V. Understanding Platinum Ionomer Interface Properties of Polymer Electrolyte Fuel Cells. *J. Electrochem. Soc.* **2022**, *169* (6), 064512.
(47) Lazaridis, T.; Gasteiger, H. A. Pt-Catalyzed Oxidation of PEMFC Carbon Supports: A Path to Highly Accessible Carbon Morphologies and Implications for Start-Up/Shut-Down Degradation. *J. Electrochem. Soc.* **2021**, *168* (11), 114517.
(48) Sharma, R.; Andersen, S. M. An Opinion on Catalyst Degradation Mechanisms during Catalyst Support Focused Accelerated Stress Test (AST) for Proton Exchange Membrane Fuel Cells (PEMFCs). *Appl. Catal. B: Environ.* **2018**, *239*, 636−643.
(49) Ferreira, P. J.; la O, G. J.; Shao-Horn, Y.; Morgan, D.; Makharia, R.; Kocha, S.; Gasteiger, H. A. Instability of Pt/C Electrocatalysts in Proton Exchange Membrane Fuel Cells: A Mechanistic Investigation. *J. Electrochem. Soc.* **2005**, *152* (11), A2256.
(50) Dam, A. P.; Abuthaher, B. Y. A.; Papakonstantinou, G.; Sundmacher, K. Insights into the Path-Dependent Charge of Iridium Dissolution Products and Stability of Electrocatalytic Water Splitting. *J. Electrochem. Soc.* **2023**, *170* (6), 064504.
(51) Đukić, T.; Moriau, L. J.; Klofutar, I.; Šala, M.; Pavko, L.; González López, F. J.; Ruiz-Zepeda, F.; Pavlišič, A.; Hotko, M.; Gatalo, M.; Hodnik, N. Adjusting the Operational Potential Window as a Tool for Prolonging the Durability of Carbon-Supported Pt-Alloy Nanoparticles as Oxygen Reduction Reaction Electrocatalysts. *ACS Catal.* **2024**, *14* (6), 4303−4317.

https://doi.org/10.1021/acsaem.5c00184
ACS Appl. Energy Mater. 2025, 8, 7939−7947